Failure mode maps for glass fibre-reinforced polymer/polyvinyl chloride foam-cored sandwich structures

Edwin Cheruiyot Kosgey
Department of Mechanical Engineering, Durban University of Technology – Steve Biko Campus, Durban, South Africa and Industrial and Energy Engineering Department, Faculty of Engineering and Technology, Egerton University, Njoro, Kenya, and
Krishnan Kanny and Festus Maina Mwangi
Department of Mechanical Engineering, Durban University of Technology – Steve Biko Campus, Durban, South Africa

Abstract

Purpose – This study aims to understand how the facesheet size, orientation and core size influence the analytical failure mechanism mode of glass fibre reinforced polymer (GFRP)/polyvinyl chloride (PVC) sandwich structures subjected to three-point bending. The purpose of this study was to develop failure-mode map of GFRP/PVC sandwich structures. Sandwich structures with different facesheet and core thicknesses were used to develop the failure map.

Design/methodology/approach – The sandwich structure and facesheet were fabricated using a vacuum-assisted resin infusion method with core sizes of 10, 15 and 20 mm and facesheet thicknesses of 1.5 and 3 mm and were arranged in three different orientations: angle-ply, cross-ply and quasi-isotropic. The key failure modes that occur in sandwich structures were used to predict possible failures in the developed material. Analytical equations were used in MATLAB for each observed failure mode. The probable failure modes, namely, face yielding, core shear and indentation equations, were used to construct the failure maps and were compared with the experimental data.

Findings – The boundary of the two failure modes shifts with changes in the facesheet and core thicknesses. The theoretical stiffness of sandwich panels was higher than the experimental stiffness. Based on strength-to-weight ratio, specimens E10-4, A15-8 and E20-8 exhibited the best optimum values owing to their shorter distance to the boundary lines.

Originality/value – In this study, a failure map was used to predict the possible failure modes for different GFRP facesheet orientations and thicknesses and PVC core thickness sandwich structures. Little is known about the prediction of the failure modes of unidirectional GFRP arranged in different orientations and thicknesses and PVC core thicknesses for sandwich structures. Few studies have used failure mode maps with unidirectional GFRP oriented in angle-ply, cross-ply and quasi-isotropic directions as a facesheet for sandwich structures compared to bidirectional mats. This study can serve as a guide for the correct selection of materials during the design process of sandwich structures.

Keywords Sandwich structures, Facesheet thickness, Core thickness, Failure map, Strength-to-weight ratio

Paper type Research paper

1. Introduction

A sandwich panel consists of a low-density core placed between two stiff and thin facesheets. The role of the core is to reinforce the facesheets during the out-of-plane properties, provide strength against indentation and buckling and resist shear forces (Mirsalehi *et al.*, 2024). Sandwich structures are widely applied in engineering fields such as marine, automotive and civil construction (Li *et al.*, 2023; Xie *et al.*, 2024; Palomba *et al.*, 2022; Mater *et al.*, 2024; Prabhu *et al.*, 2023a; Prabhu *et al.*, 2023b; Prabhu *et al.*, 2024) because of their excellent response to bending forces. Several core types are employed in sandwich structures, categorized as corrugated cores, honeycomb cores, foam cores, lattice cores and origami cores, where they exhibit different failure modes (Ma *et al.*, 2021; Feng *et al.*, 2020).

Foam cores, such as polyvinyl chloride (PVC), are often used because of their low weight and high energy absorption (Imielińska *et al.*, 2008). Foam-cored sandwich structures

The current issue and full text archive of this journal is available on Emerald Insight at: **https://www.emerald.com/insight/1708-5284.htm**

World Journal of Engineering
Emerald Publishing Limited [ISSN 1708-5284]
[DOI 10.1108/WJE-03-2024-0147]

The authors acknowledge Durban University of Technology research office for postgraduate support finances.

Availability of data and materials: The data sets used during the current study are available from the corresponding author upon reasonable request.

Competing interests: The authors declare that they have no competing financial interests or personal relationships that could have appeared to influence the work reported in this paper.

Received 28 March 2024
Revised 27 April 2024
Accepted 28 May 2024

exhibit failure modes, namely, face yield, face wrinkling, core shear, debonding and indentation (Valenza *et al.*, 2010; Liu *et al.*, 2022). The occurrence of these failure modes in bending can be predicted using the failure mode maps. Failure maps play an essential role in the design of sandwich panels, owing to the probable failure modes that provide a benchmark for designing lightweight structures (Xie *et al.*, 2024; Zhang *et al.*, 2022). The goal in using failure map is to ascertain the correlation between the failure mode and design configuration for particular loading parameters, facesheets and core properties (Triantafillou and Gibson, 1987). When two failure modes co-occur, the failure equations are equated to the two modes that provide the boundary equation (Triantafillou and Gibson, 1987; Kotzem *et al.*, 2021). This boundary equation is then used to plot a graph using axes to represent the design configuration for each failure mode (Triantafillou and Gibson, 1987; Xie *et al.*, 2024).

Failure mode maps are developed based on the core and facesheet properties. Several studies have been conducted to elaborate on the failure maps. Yuan *et al.* (2022) studied the failure behaviour of double-layer aluminium of 0.5–3 mm facesheet thickness and 5–25 mm core thickness aluminium. The authors reported that, for a high facesheet thickness, the critical failure mode of the double-layered sandwich panel was core shear, while the low ratio of core thickness to span length led to face yield failure. Xie *et al.* (2024) studied the failure modes of curved sandwich beams with a 25 mm core thickness and 2.4 mm facesheet thickness. The authors reported that the parametric analysis of panel with cross-ply fibre angle layup had the highest stiffness 0.38 kN/mm while angle-ply fibre layup had the lowest stiffness at 0.31 kN/mm with local indentation failure.

Ávila (2007) studied the failure mode of functionally graded polystyrene cores with different densities and thicknesses. The authors reported that yielding occurred regardless of the core layer stacking sequence. Valenza *et al.* (2010) developed a failure mode map for glass fibre reinforced polymer (GFRP)/PVC sandwich panels with various span lengths and facesheet thicknesses. The developed theoretical model predicted the experimental failure modes of types I and II core shear and facesheet failure in the tension mode. Steeves and Fleck (2004b) and Steeves and Fleck (2004a) studied the collapse mechanism of sandwich panels of PVC/GFRP and identified three dominant failure mechanisms: face yielding, core shear and indentation. The authors optimized the geometry by constructing a failure map and deduced the minimum weight as a function of the structural load index. Vitale *et al.* (2017) studied the mechanical behaviour and failure mode of natural fibre honeycomb and PVC core reinforced by jute and glass fibre facesheet sandwich panels under three-point bending. The authors reported that the failure map indicated different dominant failure modes: core crushing, face wrinkling, core shear and debonding.

From the discussed literature, information still needs to be included in the influence of unidirectional glass fibre orientations when combined with different facesheet and core thicknesses to predict the failure mode using a failure map. This study aims to understand how the facesheet size, orientation and core size influence the failure mechanism mode of GFRP/PVC sandwich structures subjected to three-point bending. The present failure modes of GFRP as a facesheet are available in the literature. However, little information is available about predicting the failure modes of unidirectional GFRP arranged in different orientations and thicknesses on one hand and PVC core thicknesses for sandwich structures on the other. Few studies have used failure mode maps with unidirectional GFRP oriented in angle-ply, cross-ply and quasi-isotropic directions as a facesheet for sandwich structures compared to bidirectional mats. Information on the predicted failure modes in sandwich structures serves as a guideline for academicians, engineers and designers during the development and optimization of materials for structures using GFRP and PVC, such as boats and wind turbine blades.

2. Analytical modelling of three-point bending behaviour of sandwich panel

The failure load of the sandwich panel under a quasi-static flexural test was predicted based on the mechanical properties of the core and facesheet. The assumption is that the facesheet behaves linearly and fails according to the classical beam theory (Mostafa *et al.*, 2014). Consider a simply supported sandwich panel in three-point bending mode with a uniform cylindrical roller, shown in Figure 1. The central section of the sandwich panel moves by deflection u because of the applied load P in the loading roller. Let L be the sandwich panel separation distance between the two supports, b the width of the beam, H the overhang at each end, t_f the face thickness and t_c the core thickness. The important mechanical properties of the core are the Young's modulus E_c, the compression strength σ_c, shear strength τ_c and shear modulus G_c. The mechanical properties of the facesheet include yield strength σ_f and the axial Young's modulus E_f (Steeves and Fleck, 2004b). The load of the different failure modes can be calculated using the mechanics of the materials formula. The likely failure modes for foam-cored sandwich structures are face yielding, core shear failure, indentation, debonding and face wrinkling (Mostafa *et al.*, 2014).

2.1 Stiffness

The overall deflection u at the central location of a simply supported sandwich panel loaded in three-point bending is given as the sum of the deflections caused by the bending of the facesheets and the shear of the core (Steeves and Fleck, 2004b):

$$u = \frac{PL^3}{48(EI)_{eq}} + \frac{PL}{4(AG)_{eq}} \quad (1)$$

where $(EI)_{eq}$ is the equivalent flexural rigidity, $(AG)_{eq}$ is the equivalent shear rigidity and $d = t_c + t_f$ is the distance between the centroids of the faces:

Figure 1 Geometrical parameters of a sandwich panel as loaded in three-point bending test

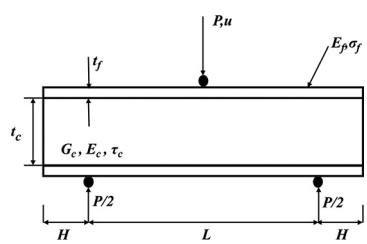

Source: Steeves and Fleck (2004b)

$$(EI)_{eq} = \frac{E_f b t_f d^2}{2} + \frac{E_f b t_f^3}{6} + \frac{E_c t_c^3}{12} \approx \frac{E_f b t_f d^2}{2} \quad (2)$$

$$AG_{eq} = \frac{bd^2}{t_c} G_c \approx b t_c G_c \quad (3)$$

2.2 Strength

In sandwich structures, the primary failure modes include face yield, face wrinkling, core shear and indentation (Steeves and Fleck, 2004b; Allen, 2013). Facesheet failure occurs when the axial compressive/tensile stress of facesheet exceeds its maximum strength. The failure of the sandwich structure resulted from compression failure in the upper facesheet. From the classical theory of sandwich panels, the axial strain is assumed to exhibit linear variation over the cross-section of the panel, as in the case of the Euler–Bernoulli theory (Mostafa *et al.*, 2014). Failure by indentation is more challenging and is dealt with as a particular case (Steeves and Fleck, 2004b). For the four failure modes, the relevant predicted failure loads are as follows:

2.2.1 Face yielding or micro buckling

Face yielding occurs when the critical stress of the facesheets reaches the yield stress of the facesheet material (Zhang *et al.*, 2022). The facesheet is considered to be elastic perfectly plastic, and face yield occurs only when the facesheets reach total plastic deformation. Shear stress in the facesheets are negligible compared with the normal stresses σ_f; hence, the equivalent stress is equal to the normal stress (Triantafillou and Gibson, 1987). The threshold load just before onset of failure of a sandwich beam is given by Steeves and Fleck (2004b):

$$P_{fy} = \frac{4\sigma_f b d t_f}{L} \quad (4)$$

2.2.2 Core shear failure

The bending moment on a sandwich structure is mainly carried by front and back facesheets, while the transverse shear force is mainly carried by core (Zhang *et al.*, 2020). Core shear occurs when the thickness of the facesheet is relatively small compared to that of the core. Thus, core shear failure is assumed to occur at a uniform shear strength with negligible additional strength of the facesheets (Steeves and Fleck, 2004a). The threshold loads necessary to cause core shear damage is given by:

$$P_{cs} = 2\tau_c b d \quad (5)$$

2.2.3 Face wrinkling

In facesheet wrinkling mode, it is assumed that the top facesheet and the upper surface of the foam core undergo the same deformation in the y-direction when wrinkling occurs in the top facesheet. The top facesheet buckles in a wrinkle-like manner when the normal stress σ_f in the facesheet reaches the critical stress (Omachi *et al.*, 2020). Thus, the face wrinkling is described as localized unstable elasticity of the facesheet contributed by short wavelength elastic buckling of the upper facesheet that does not match the wavelength of the underlying elastic core (Steeves and Fleck, 2004a). The face-wrinkling threshold load is given by:

$$P_{fw} = \frac{2bt_f(t_f + t_c)}{L} \sqrt[3]{E_f E_c G_c} \quad (6)$$

2.2.4 Indentation

Indentation refers to a specific local mode of failure that is often observed in sandwich structures with thicker cores and thinner facesheets. This form of failure occurs jointly with plastic deformation and core yield, marking a notable advancement in material stress transfer (Jin *et al.*, 2023). The indentation of sandwich structures occurs by the plastic yield of the core with facesheets deforming either elastically or plastically, as discussed in detail by Steeves and Fleck (2004a). The assumption is that the facesheet maintains an elastic state during the indentation scenario, and the core assumes a rigid, perfectly plastic solid. Hence, the minimum load is given by:

$$P_I = 2bt_c \left(\frac{\pi^2 \sigma_c^2 E_f d}{3L} \right)^{1/3} \quad (7)$$

3. Experiment

3.1 Materials and fabrication

3.1.1 Materials

The sandwich structures used in this study comprised a PVC polymeric foam core and unidirectional (UD) glass fibres of 500 gsm. Core thicknesses of 10, 15 and 20 mm with a density of 80 kg/m^3 were used. The fibres were arranged to form different stacking sequences and orientations, keeping ply numbers as four and eight layers to ensure a uniform facesheet thickness. The technical material properties of the core obtained from the manufacturer are listed in Table 1. The chemicals used were LR30 epoxy resin and LH30 slow hardener mixed at a ratio of 100:25 by weight for the resin to hardener. LR30 epoxy resin and LH30 hardener have low viscosity and are suitable for the vacuum infusion process. This mixture was designed to exhibit excellent toughness and mechanical properties after post curing. All materials and chemicals used were purchased from AMT composites, Durban.

3.1.2 Fabrication

The specimens were fabricated using LR30 epoxy resin and LH30 slow hardener using the vacuum-assisted resin infusion

Table 1 Mechanical properties of PVC foam core

Density	Compressive strength	Compressive modulus	Shear strength	Shear modulus	Tensile strength	Tensile modulus
ASTM D1622	ASTM D1621-10	ASTM D1621-10	ASTM C273	ASTM C273	ASTM D1623	ASTM D1623
80 kg/m^3	1.60 MPa	74 MPa	1.20 MPa	30 MPa	2.74 MPa	176 MPa

Source: Table courtesy of Kosgey *et al.* (2024), https://creativecommons.org/licenses/by/3.0/

method (VARIM). First, the weight of the fibres was measured using a digital weighing scale. Then, the required LR30 resin and LH30 slow hardener were calculated using a ratio 100:25 by weight of the fibres. The fibres were then laid in the mould with the core ready for infusion. Finally, LR30 and LH30 were mechanically stirred in a glass beaker and placed at the suction point of the infusion assembly. The suction point was clamped when all the mixtures were used and left for 24 h before demoulding. The specimens for the tensile test were made of GFRP only, whereas the sandwich structure for the three-point bend (3PB) included the foam core. The production process of the sandwich structures is shown in Figure 2.

The manufactured sandwich samples were post-processed in an oven, with the maximum temperature maintained at 80°C for 4 h. The samples were produced as panels and cut to the required sizes using a band saw with a diamond blade, as per the ASTM standard for the respective tests. In the current study, samples containing cross-ply (0/90), angle-ply (+45/−45) and quasi-isotropic glass-fibre-oriented facesheet and PVC foam cores of various thicknesses were marked for identification with notations and thickness sizes. For example, A20-4 means "A" for angle-ply orientation, "20" for core size (mm), "4" to indicate 4 layers of plies and 8 to indicate 8 layers of plies. A similar notation was "C" for cross-ply and E represents quasi-isotropic orientation.

3.2 Tensile test

Tensile properties were conducted for the facesheet only. These properties were used during the formulation of the boundary lines as they help in the prediction of the possible failure modes. The tensile tests of the fibre composite facesheet were carried out following (ASTMD3039/D3039M, 2000) standard. The ends of the specimen were carefully clamped at the gripping area to avoid slippage that can result in premature failure. The specimens were tested at test rate of 1 mm/min in tension using MTS Criterion, Model 43, an electronic universal testing machine installed with a load cell capacity of 30 kN. The test rate of 1 mm/min was chosen after testing other rates following ASTM D3039 standard where constant strain rate in gage section has to occur between 1 and 10 min. The tensile stresses and strains were calculated based on the load and displacement data obtained from the raw data. Table 2 shows tensile test data (yield strength and Young's modulus) for GFRP facesheet.

Figure 2 Vacuum infusion process

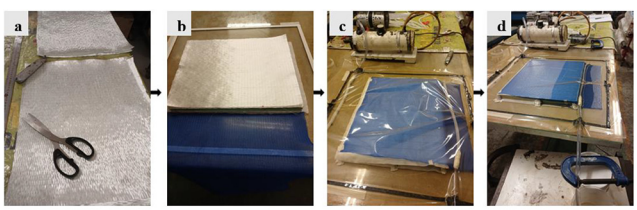

Notes: (a) Preparation of fibres, (b) laying of fibres in the mould, (c) complete setup of mould and (d) infusion of epoxy resin
Source: Authors' own work

3.3 Three-point bending experiments

A three-point bending test was performed in universal testing machine MTS Model 43 equipped with 30 kN load cell at test rate of 3 mm/min as per ASTMC393/C393M (2020). Similar standard was used by Xie *et al.* (2024) for three-point bending test of sandwich panels. The lengths of the sandwich specimens were 200 mm, width of 60 mm and span length was maintained at 150 mm. The support and loading bars were steel cylinders with diameters of 25 mm. The data were captured using the data acquisition system software, which records the load against the corresponding displacement. The peak of the load–displacement curve was considered as the critical load failure point.

4. Failure maps construction

Numerous factors influence the failure load and failure mechanisms of sandwich panels as discussed in the analytical section. The failure mode is determined by the properties of the facesheet and core materials, such as orientation of the facesheet, thicknesses of the facesheet and core, and span length. The failure map mechanism was constructed following the methodologies described in (Steeves and Fleck, 2004b; Słonina *et al.*, 2023). Failure mode maps were developed using MATLAB (MathWorks, 2023b). The sandwich beam failure load depends on the properties of the facesheet (E_f, t_f), core thickness (E_c, t_c) and span length L (mm). The failure mode maps are represented by a graph that shows the possible failure modes. Boundaries were used to represent zoning for the different failure modes. The critical load on the sandwich panel is considered as a function of the material properties and geometric parameters of the material. To obtain boundaries for various failures for stresses in facing and core, equations (4)(5), (5)(7) and (4)(7) were compared side by side and corresponding relations were obtained as shown in equations (8)–(10).

For core shear versus face yield (CS/FY):

$$\frac{t_f}{L} = \frac{1}{2} * \frac{\tau_c}{\sigma_f} \tag{8}$$

Table 2 Tensile properties of GFRP facesheet

Structural variables	Young's modulus, E_f (GPa)	Yield strength, σ_f (MPa)
A4	2.62	77.99
C4	9.33	396.36
E4	7.07	197.43
A8	2.84	122.42
C8	17.60	296.59
E8	10.32	338.93

Source: Table courtesy of Kosgey *et al.* (2024), https://creativecommons.org/licenses/by/3.0/

For face yield versus indentation (FY/I):

$$\frac{t_c}{L} = 2\sigma_f d * L^{3/2}\left(\frac{3}{\pi^2\sigma_c^2 E_f d}\right)^{1/3} * \frac{t_f}{L} \quad (9)$$

For core shear versus indentation:

$$\frac{t_c}{L} = \left(\frac{3\tau_c^3 d^2}{\pi^2\sigma_c^2 E_f L^2}\right)^{1/3} \quad (10)$$

5. Results and discussion

5.1 Failure mechanisms

The constructed failure maps for panels with facesheets of various thicknesses, ply-orientations and core thicknesses, based on the analytical parameters elaborated in Section 2. The failure maps do not indicate the failure load of the sandwich panel; rather, they indicate the possible failure mode that will occur.

The failure mode maps constructed from the geometrical dimensions of the materials are illustrated in Figures 3 and 4, showing the simultaneous curves for core sizes of 10, 15 and 20 mm. From Figures 3 and 4, it can be observed that the face yield and indentation occupy the largest area of the map, whereas core shear occurs only in a limited area. A possible reason for this behaviour is that the breaking loads of the face yield and indentation are functions of the material properties of the facesheet. Furthermore, the PVC foam core has good resistance to shear compared to the GFRP facesheet, which contributes to the small area of the core shear failure. The face yield is dominant in regions with high values of t_c/L and t_f/L. This scenario can be explained by considering that, for this geometrical configuration, the indentation of the upper

Figure 3 Failure mode maps for sandwich structures with 1.5 mm facesheet and different core thicknesses

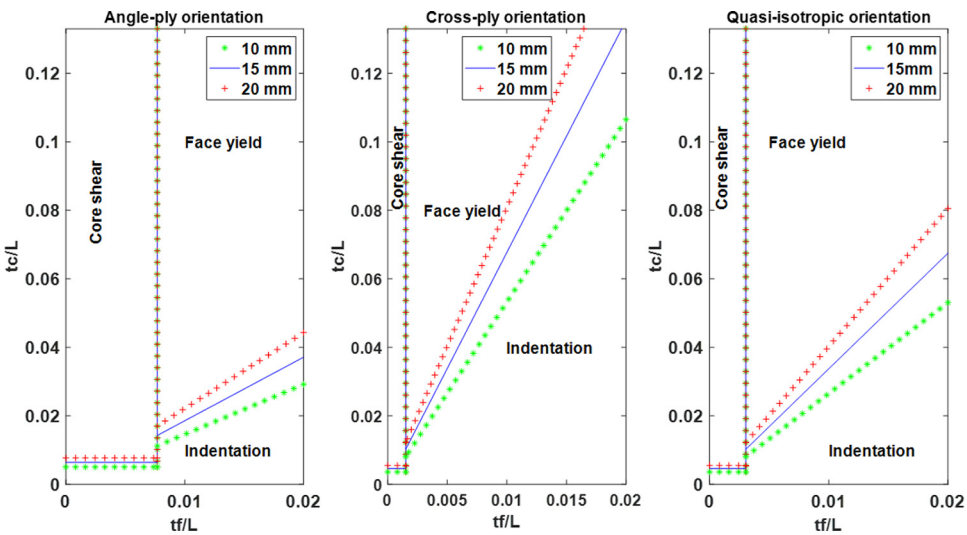

Source: Authors' own work

Figure 4 Failure mode maps for a 3 mm facesheet depicting different core thicknesses

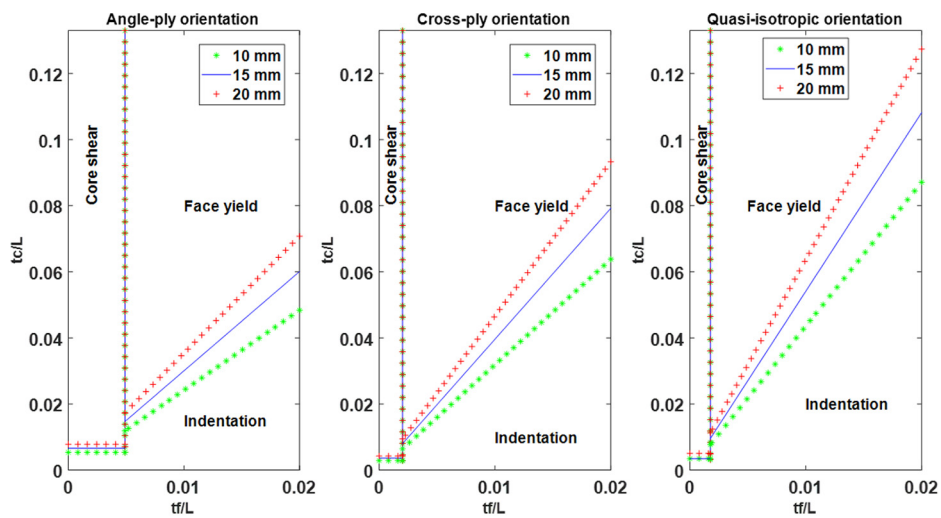

Source: Authors' own work

facesheet increases, which prevents premature indentation failure. Moreover, stress is applied onto the weaker areas of the sandwich panels, which causes the axial stress to exceed the tensile strength of the facesheet.

A three-point bending test was conducted with different combinations of the facesheet and core at a constant span length, and failure modes were identified. Figure 5 shows the failure modes obtained from the three-point bend experiment conducted on the GFRP/PVC sandwich panel. The dominant failure modes of indentation, face yield and core shear, which were analysed in Section 2, are visible. Specimen E10-4 exhibited face yield failure in the experiment, which was well predicted by the failure map shown in Figure 3. This result was replicated well in all other facesheet orientations with similar core sizes and facesheet thicknesses. Specimens C20-4 and E20-8 exhibited indentation failure. The thickness of the core contributes to indentation, as the loading roller leads to the densification of the PVC foam cells, thereby creating a local indent at that point.

Figure 5 Failure modes

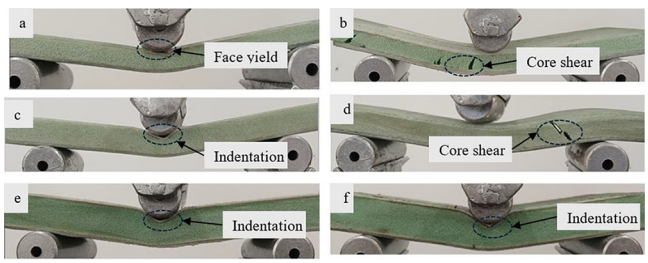

Notes: (a) E10-4; (b) C10-8; (c) A15-4; (d) C15-8; (e) C20-4; (f) E20-8 selected samples as observed in quasistatic three-point bending
Source: Authors' own work

5.2 Load carrying capacity

Table 3 shows a summary of the experimental results, where P_{max} is the maximum load, and D_{exp} and D_{the} are the experimental and theoretical elastic bending stiffnesses, respectively. D_{exp} was obtained from the experimental data, as follows:

$$D_{\exp} = \frac{\Delta P}{\Delta \delta} \tag{11}$$

where ΔP and $\Delta\delta$ are the increment of the load and the corresponding displacement from the test data, respectively. The theoretical elastic bending stiffness can be obtained from equations (1)–(3). From Table 3, it can be observed that the theoretical prediction of the elastic bending stiffness was higher than the experimental results. The likely reason is that the theoretical analysis considered the interaction between the facesheet and core. Furthermore, the adhesive used during the laboratory production of the sandwich panel was very thin, which had little effect on the load capacity. Finally, the orientation of the fibres in the facesheet laminate contributed to a higher theoretical stiffness for the cross-ply and quasi-isotropic orientations than for the angle-ply orientation. A contrary result was reported by (Li *et al.*, 2014), where the theoretical bending stiffness values were lower than the experimental bending stiffness values for aluminium foam at elevated temperatures.

5.3 Optimization of structural variables

Table 4 shows the distances of the structural variables to the intersection point. The distance from the location of the structural variables to the intersection point was calculated using the formula used to calculate the distance between two points in a plane. Specimens near the boundary line possess optimum structural variables because the failure modes in the core and facesheet occur simultaneously, which indicates that no excess material is utilized in the sandwich structure. Therefore, the intersection points of the boundary lines are most important (Hao *et al.*, 2020). The obtained distance was

Table 3 Geometrical parameters of sandwich panels

Structural variables	L (mm)	t_f (mm)	t_c (mm)	t_f/L	t_c/L	P_{max} (kN)	P_{fy} (kN)	P_{cs} (kN)	P_{in} (kN)	D_{exp} (N/mm)	P_{the} (N/mm)
A10-4	150	1.5	10	0.01	0.067	1.43	2.15	1.656	20.46	159.53	171.69
C10-4	150	1.5	10	0.01	0.067	1.67	10.94	1.656	31.26	231.97	355.26
E10-4	150	1.5	10	0.01	0.067	1.44	5.45	1.656	28.49	286.28	312.08
A10-8	150	3.0	10	0.02	0.067	1.52	7.64	1.872	21.90	214.40	356.91
C10-8	150	3.0	10	0.02	0.067	3.10	18.51	1.872	40.23	301.94	671.13
E10-8	150	3.0	10	0.02	0.067	1.83	21.15	1.872	33.67	354.22	598.62
A15-4	150	1.5	15	0.01	0.1	1.18	3.08	2.376	34.62	384.11	317.54
C15-4	150	1.5	15	0.01	0.1	1.38	15.70	2.376	52.88	398.38	572.83
E15-4	150	1.5	15	0.01	0.1	1.20	7.82	2.376	48.20	285.71	517.83
A15-8	150	3.0	15	0.02	0.1	1.82	10.58	2.592	36.61	298.26	562.61
C15-8	150	3.0	15	0.02	0.1	2.87	25.63	2.592	67.29	297.77	909.50
E15-8	150	3.0	15	0.02	0.1	1.30	29.28	2.592	56.30	238.39	838.67
A20-4	150	1.5	20	0.01	0.133	1.50	4.02	3.096	50.42	518.03	489.46
C20-4	150	1.5	20	0.01	0.133	1.79	20.45	3.096	77.01	663.19	799.73
E20-4	150	1.5	20	0.01	0.133	1.71	10.19	3.096	70.19	301.55	736.78
A20-8	150	3.0	20	0.02	0.133	1.68	13.52	3.312	52.97	536.44	781.49
C20-8	150	3.0	20	0.02	0.133	3.04	32.74	3.312	97.31	631.27	1148.90

Source: Table by authors

Table 4 Summary of the distances from structural variables to intersection points

Structural variables	t_f/L	t_c/L	P_{max} (kN)	Density (kg/m^3)	Strength-to-weight ratio (N m/kg)	Distance to intersection
A10-4	0.01	0.067	1.43	543.48	74,493.67	0.0558
C10-4	0.01	0.067	1.67	547.10	86,506.99	0.0595
E10-4	0.01	0.067	1.44	586.96	69,632.44	0.0593
A10-8	0.02	0.067	1.52	730.77	46,093.07	0.0572
C10-8	0.02	0.067	3.10	753.21	91,395.81	0.0632
E10-8	0.02	0.067	1.83	833.33	48,717.35	0.0618
A15-4	0.01	0.1	1.18	478.32	70,135.60	0.0856
C15-4	0.01	0.1	1.38	488.87	80,181.82	0.0898
E15-4	0.01	0.1	1.20	451.92	75,380.96	0.0923
A15-8	0.02	0.1	1.82	663.99	31,687.99	0.0866
C15-8	0.02	0.1	2.87	626.74	52,956.27	0.0937
E15-8	0.02	0.1	1.30	681.14	22,030.40	0.0922
A20-4	0.01	0.133	1.50	363.66	33,397.17	0.1160
C20-4	0.01	0.133	1.79	413.25	35,153.16	0.1211
E20-4	0.01	0.133	1.71	393.86	35,233.92	0.1210
A20-8	0.02	0.133	1.6764	573.01	20,739.15	0.1217
C20-8	0.02	0.133	3.0393	609.88	35,326.84	0.1248
E20-8	0.02	0.133	2.6203	601.54	30,878.92	0.1231

Source: Table by authors

used to compute the level of optimization of the strength-to-weight ratio. The strength-to-weight ratio of the sandwich panel was calculated using equation (12) (Hao *et al.*, 2020):

$$W_t = \frac{1}{\rho}\frac{3P_{max}L}{2bd^2} \tag{12}$$

Where W_t is the strength-to-weight ratio, ρ is the density of the sandwich panel, L is the span length, b is the width of the specimen and d is the mid-plane distance.

Taking A10-4 as an example, $P_{max} = 1{,}427.8$ N, $b = 0.06$ m, $L = 0.15$ m, $\rho = 555.56$ kg/m^3, $d = 0.0115$ m, thus $W_t = 74{,}493.67$ N m/kg as calculated from equation (12).

Figure 6 shows a concise pattern in which the strength-to-weight ratio of the sandwich structure is inversely proportional to the distance from the point of the structural variables to the intersection of the failure boundary line. Specimens E10-4, A15-8 and E20-8 had the best strength-to-weight ratio and shortest distance to the boundary line. On the other hand, specimens C10-8 and A20-8 had lower strength-to-weight ratios and larger distances to boundary lines.

Figure 6 Relationship between strength-to-weight ratio of sandwich structure and distance from point of structural variables to intersection point

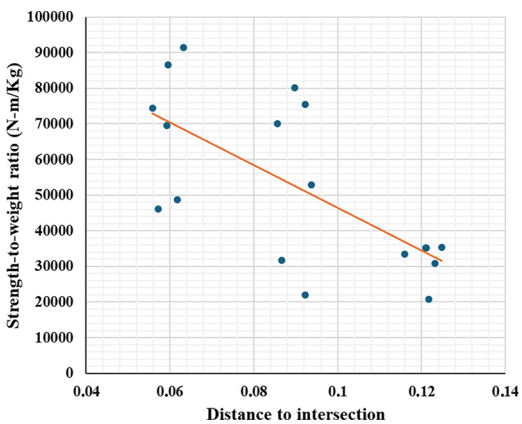

Source: Authors' own work

6. Conclusion

This study focusses on the analytical failure modes of GFRP/PVC sandwich panels under a three-point bending load. The failure mode map was developed to predict the failures in sandwich panels for the relationship between the facesheet thickness, core thickness, and span length between the loading supports. The facesheet thickness of 1.5 and 3 mm, and core thickness of 10, 15 and 20 mm were used for design. From the experiments used for validation, three failure modes were dominant: face yield, indentation and core shear. For the maximum load carrying capacity, the theoretical stiffness was higher than experimental stiffness by 42.23%. These failure modes are expressed in a failure mode map on the graph of t_c/L versus t_f/L. The information from the failure map was used to compute the strength-to-weight ratio of the sandwich composite to optimize the structural parameters and ensure minimal wastage of the materials. The strength-to-weight ratio varied from 20,739.15 to 91,395.81 N m/kg, whereas distance to intersection varied from 0.0558 to 0.1248. It was observed that specimens with the shorter distance to boundary lines gave the best results. The analytical model developed showed results consistent with the experimental data, thus indicating a reliable tool to predict failure mechanisms in sandwich structures.

This study can be extended to failure mode maps using quasi-static indentation and dynamic tests such as low-velocity impact. Currently, the authors are working on analytical and experimental research on failure modes of impact energy

propagation for GFRP/PVC sandwich panels. Furthermore, with disruptive technology, sandwich structures can be fabricated using 3D printing in continuous and discontinuous methods, using materials with a density equivalent to PVC for comparison.

References

Allen, H.G. (2013), *Analysis and Design of Structural Sandwich Panels: The Commonwealth and International Library: structures and Solid Body Mechanics Division*, Elsevier, New York, NY.

ASTMC393/C393M (2020), "Standard test method for core shear properties of sandwich constructions by beam flexure".

ASTMD3039/D3039M (2000), "Tensile test method for tensile properties of polymer matrix composite materials".

Ávila, A.F. (2007), "Failure mode investigation of sandwich beams with functionally graded core", *Composite Structures*, Vol. 81 No. 3, pp. 323-330.

Feng, Y., Qiu, H., Gao, Y., Zheng, H. and Tan, J. (2020), "Creative design for sandwich structures: a review", *International Journal of Advanced Robotic Systems*, Vol. 17 No. 3, p. 172988142092132.

Hao, J., Wu, X., Oporto, G., Liu, W. and Wang, J. (2020), "Structural analysis and strength-to-weight optimization of wood-based sandwich composite with honeycomb core under three-point flexural test", *European Journal of Wood and Wood Products*, Vol. 78 No. 6, pp. 1195-1207.

Imielińska, K., Guillaumat, L., Wojtyra, R. and Castaings, M. (2008), "Effects of manufacturing and face/core bonding on impact damage in glass/polyester–PVC foam core sandwich panels", *Composites Part B: Engineering*, Vol. 39 No. 6, pp. 1034-1041.

Jin, Z., Mao, W. and Yang, F. (2023), "Failure analysis of sandwich beams under three-point bending based on theoretical and numerical models", *Science and Engineering of Composite Materials*, Vol. 30 No. 1, p. 20220224.

Kosgey, E.C., Kanny, K. and Mwangi, F.M. (2024), "Mechanical behaviour of glass fibre-reinforced polymer/polyvinyl chloride foam cored sandwich structures", *Advances in Materials Science and Engineering*, Vol. 2024, p. 5929170.

Kotzem, D., Tazerout, D., Arold, T., Niendorf, T. and Walther, F. (2021), "Failure mode map for E-PBF manufactured Ti6Al4V sandwich panels", *Engineering Failure Analysis*, Vol. 121, p. 105159.

Li, Z., Gao, Y., Wang, Y., Xue, P., Gong, C., Wang, W., Wei, X. and Xiong, J. (2023), "Failure mechanisms and acoustic emission pattern recognition of all-CFRP cylindrical honeycomb sandwich shell under three-point bending", *Composites Science and Technology*, Vol. 237, p. 110003.

Liu, H., Liu, J., Kaboglu, C., Zhou, J., Kong, X., Li, S., Blackman, B.R., Kinloch, A.J. and Dear, J.P. (2022), "Modelling the quasi-static flexural behaviour of composite sandwich structures with uniform-and graded-density foam cores", *Engineering Fracture Mechanics*, Vol. 259, pp. 108-121.

Li, Z., Zheng, Z., Yu, J., Qian, C. and Lu, F. (2014), "Deformation and failure mechanisms of sandwich beams under three-point bending at elevated temperatures", *Composite Structures*, Vol. 111, pp. 285-290.

Ma, Q., Rejab, M., Siregar, J. and Guan, Z. (2021), "A review of the recent trends on core structures and impact response of sandwich panels", *Journal of Composite Materials*, Vol. 55 No. 18, pp. 2513-2555.

Mater, Y.M., Elansary, A.A. and Abdalla, H.A. (2024), "Experimental and numerical investigation of preloaded recycled concrete beams strengthened with CFRP", *World Journal of Engineering*.

MATLAB (MathWorks, 2023), available at: www.mathworks.com/products/new_products/release2023b.html

Mirsalehi, M., Kianpour, K., Shahbeyk, S. and Bakhshi, M. (2024), "The effect of load concentration on one-way response of 3D-woven sandwich panels", *Composite Structures*, Vol. 327, p. 117659.

Mostafa, A., Shankar, K. and Morozov, E. (2014), "Experimental, theoretical and numerical investigation of the flexural behaviour of the composite sandwich panels with PVC foam core", *Applied Composite Materials*, Vol. 21 No. 4, pp. 661-675.

Omachi, A., Ushijima, K., Chen, D.-H. and Cantwell, W.J. (2020), "Prediction of failure modes and peak loads in lattice sandwich panels under three-point loading", *Journal of Sandwich Structures & Materials*, Vol. 22 No. 5, pp. 1635-1659.

Palomba, G., Epasto, G., Sutherland, L. and Crupi, V. (2022), "Aluminium honeycomb sandwich as a design alternative for lightweight marine structures", *Ships and Offshore Structures*, Vol. 17 No. 10, pp. 2355-2366.

Prabhu, R., Mendonca, S., Bellairu, P.K., D'Souza, R.C. and Bhat, T. (2023a), "Optimization of dry sliding wear performance of TiO_2 filled bamboo and flax fiber reinforced epoxy composites using Taguchi approach", *World Journal of Engineering*.

Prabhu, R., Mendonca, S., Bellairu, P.K., DSouza, R.C. and Bhat, T. (2023b), "Effect of TiO_2 filler on mechanical and tribological properties of Owen bamboo fiber reinforced epoxy composite", *World Journal of Engineering*, Vol. 21 No. 4.

Prabhu, R., Mendonca, S., Bellairu, P.K., DSouza, R.C. and Bhat, T. (2024), "Investigating the impact of TiO_2 filler on abrasive wear characteristics of bamboo fiber-reinforced epoxy composites using the Taguchi method", *World Journal of Engineering*.

Słonina, M., Dziurka, D. and Smardzewski, J. (2023), "Failure mechanism map for bending wood-based honeycomb sandwich beams with starch-impregnated core", *Composite Structures*, Vol. 310, p. 116749.

Steeves, C.A. and Fleck, N.A. (2004a), "Collapse mechanisms of sandwich beams with composite faces and a foam core, loaded in three-point bending. Part I: analytical models and minimum weight design", *International Journal of Mechanical Sciences*, Vol. 46 No. 4, pp. 561-583.

Steeves, C.A. and Fleck, N.A. (2004b), "Collapse mechanisms of sandwich beams with composite faces and a foam core, loaded in three-point bending. Part II: experimental investigation and numerical modelling", *International Journal of Mechanical Sciences*, Vol. 46 No. 4, pp. 585-608.

Triantafillou, T.C. and Gibson, L.J. (1987), "Failure mode maps for foam core sandwich beams", *Materials Science and Engineering*, Vol. 95, pp. 37-53.

Valenza, A., Fiore, V. and Calabrese, L. (2010), "Three-point flexural behaviour of GFRP sandwich composites: a failure map", *Advanced Composite Materials*, Vol. 19 No. 1, pp. 79-90.

Vitale, J.P., Francucci, G., Xiong, J. and Stocchi, A. (2017), "Failure mode maps of natural and synthetic fiber reinforced composite sandwich panels", *Composites Part A: Applied Science and Manufacturing*, Vol. 94, pp. 217-225.

Xie, H., Li, W., Fang, H., Zhang, S., Yang, Z., Fang, Y. and Yu, F. (2024), "Flexural behavior evaluation of a foam core curved sandwich beam", *Composite Structures*, Vol. 328, p. 117729.

Yuan, H., Zhang, J. and Sun, H. (2022), "The failure behavior of double-layer metal foam sandwich beams under three-point bending", *Thin-Walled Structures*, Vol. 180, p. 109801.

Zhang, W., Qin, Q., Li, J., Su, B. and Zhang, J. (2020), "A comparison of structural collapse of fully clamped and simply supported hybrid composite sandwich beams with geometrically asymmetric face sheets", *Composites Part B: Engineering*, Vol. 201, p. 108398.

Zhang, Z-J., Wei, X., Wu, K., Wang, Y-J., Jia, Z., Zhang, Q-C. and Jin, F. (2022), "Failure analysis of brazed sandwich structures with square honeycomb-corrugation hybrid cores under three-point bending", *Thin-Walled Structures*, Vol. 170, p. 108591.

Corresponding author

Krishnan Kanny can be contacted at: kannyk@dut.ac.za